Modeling Refraction Errors for Simulation Studies of Multisensor Target Tracking

J. Clayton Kerce, William D. Blair, George C. Brown
Sensors and Electromagnetic Applications Laboratory
Georgia Tech Research Institute
Georgia Institute of Technology
Atlanta, Georgia 30332 USA
clayton.kerce@gtri.gatech.edu

Key Words: radar simulation, refraction modeling, multi-sensor target tracking.

Abstract: Approximations are derived for the delay and bending of a wavefront propagating through the class of spherically symmetric refractivity profiles which decay exponentially with altitude. These approximations are derived by formulating the quantities of interest in terms of an optimization problem, the solution of which is then estimated for an appropriately chosen candidate path. Based on these approximations, a simple model is introduced to simulate the residual measurement errors remaining after the application of a notional refraction correction algorithm. The application of this model to the simulation of multi-sensor, multi-platform tracking is discussed.

I. INTRODUCTION

Natural variations in the atmospheric index-of-refraction cause bending and delay of radar and optical signals, resulting in elevation-dependent measurement biases at the sensor. These measurement biases result in biased position and velocity estimates in the track filter [1][2]. Such effects are most pronounced for targets at low elevation angles and long ranges.

The main results of this paper are approximations for the delay and bending associated with wavefront propagation through an exponential refraction profile. The approximations are expressed as simple combinations of the physical and geometric parameters as

$$\Delta\tau \approx \frac{\alpha}{c} F(\beta, L, \theta_{el}, R) \tag{1}$$

$$\theta_{bending} \approx \alpha\,\beta\cos(\theta_{el}) F(\beta, L, \theta_{el}, R) \tag{2}$$

Here the atmospheric parameter α can be expressed in terms of the temperature, pressure and humidity at the ground through the Smith-Weintraub equation. The parameter β defines the lapse rate of the refractive profile. L is the propagation distance, θ_{el} the target elevation angle, R the sensor height in Earth-Centered-Earth-Fixed coordinates (ECEF), and the function F is defined in Section II.

An important feature of these approximations is that they do not assume that the target and sensor are at the same altitude, a situation that precludes the use of 4/3 Earth type models. Instead, the range error is formulated as an optimization problem by applying Fermat's principle of least time [3]. The travel time functional is then evaluated along on a suboptimal path that is intuitively close to the true solution. A second order approximation in the exponent of the refractivity puts the cost function in the form of a Gaussian integral that can be explicitly evaluated. The bending of the true propagation path is approximated by computing the bending due to the refraction gradient along the path used in the range error calculation.

The goal of this paper is to develop a method for simulating the residual errors that remain after the application of a refraction correction algorithm in order to enable the study of refraction errors on multiple sensor network tracking of multiple targets. In this application, an individual sensor typically implements a correction algorithm to reduce the refraction induced angle-of-arrival and range errors to within a small fraction of the magnitude of the original errors. The remaining errors are a function of both the refraction model and the quality of the meteorological data used as input into the model. Assuming that both the model and the meteorological values remain constant throughout a track, the residual errors will produce a deterministic track bias in each sensor that is a function of both target range and elevation. Since the relative ranges and elevations to the targets are different for each sensor, the resulting biases will vary between sensors as well. These biases can cause significant problems when one attempts to associate tracks from multiple sensors.

The approximations obtained here are compared to the results of numerical ray-tracing, and it is found that for practical profiles the model agrees with the numerical solutions to within about ten percent for all ranges and elevations. As seen from the formulas and ray tracing comparison, the resulting residual error model has low computational overhead and captures the important phenomenology associated with the effects of regular refraction for all elevation angles.

0-7803-8281-1/04/$20.00

An example of the application of this formula to the study of track-to-track association is presented using Monte Carlo simulation. The correction residual is chosen from a Gaussian probability distribution function with variance chosen to reflect the expected accuracy of the correction algorithm of the radar. The correction factor remains constant throughout each Monte Carlo run.

This paper is organized as follows. Refraction effects and the primary application of interest are reviewed in the introduction. The second section develops the bending and delay approximations using Fermat's principle of least time for a model exponential profile. The final section presents some applications of the model with a focus on its use as a simulation tool.

II. DERIVATION OF THE FORMULA

For an inhomogeneous medium, the index-of-refraction, *n*, at a point x in the medium is related to the speed of light in the medium, *v*, and the speed of light in vacuum, *c*, by the formula $n(x) = \frac{c}{v(x)}$. With this definition, one can compute the travel time, τ, for light along an arclength-parameterized path, *x(s)*, of length *L* through the formula

$$\tau(x(\cdot)) = c^{-1}\int_0^L n(x(s))\,ds\ .$$

The principle of least time (PLT) states that among all potential paths light could take between two prescribed endpoints, the physical path corresponds to the minimizing path in the integral above*. Applying this principle, one finds that the trajectory of a light ray satisfies the equation

$$\ddot{x} = \frac{1}{n}\left[\nabla n - (\nabla n \cdot \dot{x})\,\dot{x}\right],$$

where ∇ denotes the spatial gradient and *x(s)* has initial conditions $x(0) = x_0$, $\dot{x}(0) = \dot{x}_0$, and $|\dot{x}_0| = 1$.

Before proceeding to the derivation, let the exponential atmospheric profiles be expressed as $n(x) = 1 + \alpha e^{-\beta h(x)}$. Here *h(x)* denotes the height of the point *x* above the surface of the Earth. These profiles have no variation in angle. The parameter β is the decay rate of the profile with altitude. The parameter α depends on the meteorological values at the sensor through the Smith-Weintraub equation:

$$\alpha = 10^{-6}\left(\frac{77.6\ P}{T} + \frac{3.73\cdot 10^5\ H}{T^2}\right)1,$$

where P is the pressure in millibars, T is the temperature Kelvin, and H is the partial vapor pressure of water in millibars.

We apply PLT to estimate the range and bending errors that result from the assumption of a constant speed of light *c* throughout the path. The assumption of a constant propagation speed results in the range estimation formula $R_{path} = c\ \tau$. Applying PLT along with the exponential atmosphere assumption results in a formula for the excess range error ΔR given by

$$\Delta R = \int_0^L [n(x(s)) - 1]\,ds \ = \ \alpha \int_0^L e^{-\beta h(x(s))}\,ds\ .$$

Similarly, the definition of the curvature of the path *x(s)* can be used to estimate the total bending of the ray along the path through the formula $|\kappa| = \frac{1}{n}\left|\nabla n - (\nabla n \cdot \dot{x})\,\dot{x}\right|$. Due to the assumed exponential form of *n(x)*, the derivative of the index-of-refraction with altitude is strictly negative. Making the substitution $n(x) = 1 + \alpha e^{-\beta h(x)}$, we find that the formula for the bending is

$$\theta_{bending} = \int_0^L \kappa(x(s))\ ds$$
$$= \alpha\,\beta \int_0^L \frac{e^{-\beta\,h(x(s))}}{n(x(s))}\,|\,\nabla h(x(s)) - (\nabla h(x(s))\cdot\dot{x}(s))\,\dot{x}(s)\,|\,ds. \quad (3)$$

Evaluating the integrals for bending and excess range require the evaluation of the integral $\int_0^L e^{-\beta\,h(y(s))}ds$. In order to estimate this term, the original minimization principle and the fact that the parameter $\alpha \approx 3\times 10^{-4}$, while $n \approx 1$ will be used. Because α<< *n*, the optical path is expected to be well approximated by a straight line segment joining the path endpoints. Moreover, since the optical path minimizes the travel time, the straight-line approximation will produce an upper bound on the travel time functional. Given the radar and target position vectors in a spherical earth ECEF coordinate system, $\mathbf{x}_0$ and $\mathbf{x}_1$, respectively, the explicit formulas for y(s) is $y(s) = x_0 + s\ \dot{x}_0$, where $\dot{x}_0$ is chosen so that the condition $y(L) = x_1$ is satisfied. In the plane defined by the radar, target, and earth center, *h(y(s))* can be expressed in the two coordinates and θ_{el}, where θ_{el} denotes the elevation of the target relative to the radar as $h(y(s)) = \sqrt{R_{radar}^2 + 2\,s\,R_{radar}\sin(\theta_{el}) + s^2} - R_e$, where R_e denotes the Earth's radius. Since $s \le R_e \le R_{radar}$, we expand the square root to second order in the parameter s/R_{radar} to put the integral $\int_0^L e^{-\beta\,h(y(s))}ds$ in Gaussian form. Evaluation of the resulting integral leads us to the following approximation formula, $F(\beta, L, \theta_{el}, R_{radar})$, as

* More precisely optical paths are stationary points for the travel time functional. The path examined here is assumed to be minimizing due to the small deviation of *n(x)* from unity.

$$\int_0^L e^{-\beta\, h(y(s))}\, ds \approx F(\beta, L, \theta_{el}, R_{radar})$$

$$\equiv \sqrt{\frac{\pi R_{radar}}{2\beta}}\cos(\theta_{el})\, e^{-\beta(R_{radar}-R_e)} \times e^{\beta R_{radar}\tan^2(\theta_{el})/2}\left[erf(\ell_{upper}) - erf(\ell_{lower})\right]$$

with the following parameter definitions

$$\ell_{upper} = \sqrt{\frac{\beta}{2R_{radar}}}\cos(\theta_{el}) \times \left(L + R_{radar}\sec(\theta_{el})\tan(\theta_{el})\right)$$

$$\ell_{lower} = \sqrt{\frac{\beta\ R_{radar}}{2}}\tan(\theta_{el})$$

$$erf(x) = \frac{2}{\sqrt{\pi}}\int_0^x e^{-t^2/2}\, dt\ .$$

The estimate for excess range can now be written

$$\Delta R = \alpha\, F(\beta, L, \theta_{el}, R_{radar})\ ,$$

which is easily converted to (1) using the definition of the speed of light.

The formula (3) for bending can be simplified similarly. Noticing that $\left|\nabla h(y(s))\right| = \cos(\theta_{el})$ and $n \approx 1$ gives the bending estimate

$$\theta_{bending} = \alpha\, \beta \cos(\theta_{el})\, F(\beta, L, \theta_{el}, R_{radar})\ .$$

For low elevation angles, each of the terms in the formula for $F(\beta, L, \theta_{el}, R_{radar})$ are small enough in magnitude to compute directly. As θ_{el} increases, the arguments to the exponentials and error function, *erf*, lead to numerical difficulties. In this case one can apply the approximation $erf(x) \approx 2/\sqrt{\pi}\, e^{-x^2/2}$ and simplify the expression to avoid round off errors.

Alternative approaches to modeling the refraction-induced errors were considered and the current approach is taken for a number of reasons. First, from the standpoint of Monte-Carlo simulation, the computational overhead associated with numerically computing propagation paths through complex atmospheres is significant. Secondly, more common approaches, such as the 4/3 Earth model, are only valid under fairly restrictive conditions on the target/sensor geometry [1]. Finally, alternate modeling approaches, such as characterizing the statistics of real atmospheric conditions, tend to be overly complex for understanding the effects of refraction correction errors on track-to-track association.

III. EXAMPLES

The method discussed in the previous section for computing range and bending of a wavefront by the atmosphere is approximate, and it will not work for all parameter values of α and β. Investigation over the applicable range of values for simulation evaluation of multiplatform tracking shows reasonable behavior, as indicated in the example that follows.

A. Partial Validation of Results

As a first example, the approximations (1) and (2) derived above are compared to solutions computed using numerical ray-tracing. Fig. 1 compares ray-tracing using Snell's law and the approximation for ΔR derived in the previous section as a function of slant range to the target at 0°, 1° and 5° elevation. Notice that the largest error for the approximation occurs at 0° and rapidly improves with elevation. This behavior is to be expected, since the propagation path is better approximated by a straight line for higher elevation than for lower elevation. Observe also that the approximate solutions are strictly larger than those obtained by numerical ray-tracing. This too is to be expected, since the approximation is obtained from evaluating the objective function along a sub-optimal path. The values chosen for the atmospheric parameters are P = 1000 millibars, T = 273 Kelvin, H = 15 millibars, and $\beta = 1.75\ 10^{-4}\ m^{-1}$. This β value corresponds to a 50% fall off in refractivity at about 4 km. Refractivity, N, is defined through the formula $N = 10^6(n-1)$. The meteorological parameters given correspond to a value $\alpha = 3.6\ 10^{-4}$.

Fig. 2 shows the companion plot for $\theta_{bending}$ as a function of slant range for the same elevation values. This approximation exhibits a larger deviation from the numerical ray-tracing solution because an additional approximation was made in simplifying the integral. Notice that the estimates for bending do not fall directly out of an optimization problem, and there is no a priori reason to expect that the approximation would overestimate the true solution. The consistent overestimation seen here is a consequence of the relationship between excess bending and excess range.

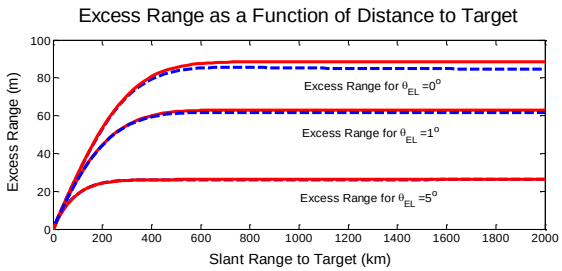

Fig. 1 Comparison of ray-tracing using Snell's law and the approximation for ΔR as a function of slant range to the target at 0°, 1° and 5° elevation. The solid line is the approximation, while the dashed line is the numerically computed curve.

The difference between computed and approximated quantities in Fig. 1 and Fig. 2 are more easily understood by

looking at percentage errors. Fig. 3 and Fig. 4 show the percent error of the approximation, e.g. the difference between the computed and approximate solutions divided by the computed solution displayed as percentages.

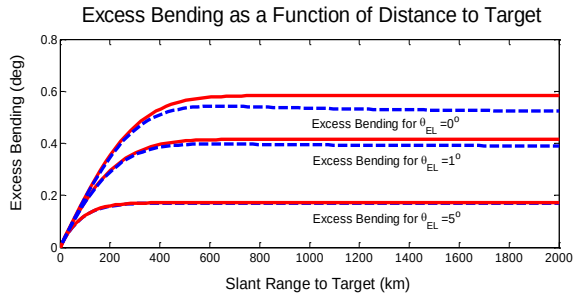

Fig. 2 Comparison of ray-tracing using Snell's law and the approximation for $\theta_{bending}$ as a function of slant range to the target at 0^o, 1^o and 5^o elevation. The solid line is the approximation; the dashed line is the numerically computed curve.

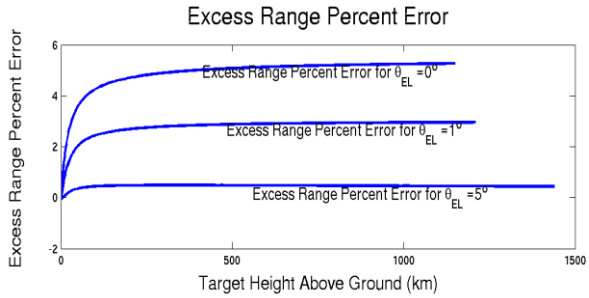

Fig. 3 Percent error of excess range approximation when compared to the excess range computed from numerical ray-tracing.

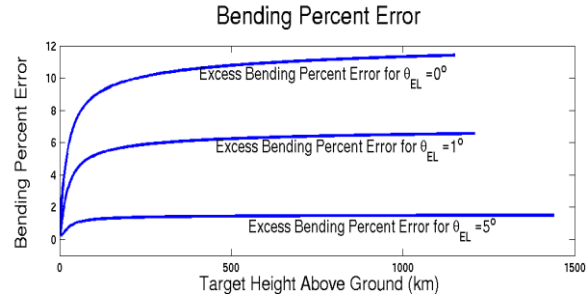

Fig. 4 Percent error of bending approximation when compared to the bending computed from numerical ray-tracing.

B. Comparison to 4/3 Earth model

These results are compared with those of a 4/3 Earth based height finding model as reported in Table 20.3, Section 20.18 of [1]. Upon converting nautical miles into kilometers and kilofeet into meters, at 0^o elevation and 550 km slant range, the 4/3 Earth model has approximately 8% error, whereas the model presented here shows approximately a 10% error for the same conditions. The relative performance of these two models changes rapidly with elevation. The 4/3 Earth model exhibits an increasing error with elevation, for instance 9% error at 0.5^o, while the error in the model presented here decreases, achieving 6% error at 1^o elevation. This discrepancy is related to the range of validity in the approximations applied to these two models. The 4/3 Earth model is based on a small order expansion around a single height, while the model presented here approximates the height along the path as a quadratic function which has an explicit dependence on target elevation. For shorter ranges the situation is similar. Comparing the 370 km slant range entries [1], one finds that the 4/3 Earth model has a slowly increasing error which starts at 4.3% for 0^o elevation and is approximately 5% for 0.5^o through 2^o. The model presented here shows 4.9% error at 0^o, 2.5% error at 1^o, and 0.5% at 5^o.

C. Refraction Effects on Track Association

As a second example, the effects of the refraction correction errors on covariance consistency are examined for the case of a single object under track by a single sensor. The sensor is a phased array radar generating monopulse AOA estimates with 15 meter range resolution. The target originates beyond the horizon and approaches the sensor. The target SNR is 20 dB, ensuring that the effects of measurement noise are negligible when compared to the refraction effects being studied. The track is formed based on an IMM estimator designed for tracking ballistic missiles. The tracking errors of 100 Monte Carlo runs was averaged to produce the results reported below.

For this example, the covariance consistency (CC) is used to measure the quality of the empirical covariance in terms of the true covariance and is defined as

$$\begin{aligned} \mathrm{CC} &= \frac{1}{N}\left\langle (\hat{x}-x)^T P^{-1} (\hat{x}-x) \right\rangle \\ &= \frac{1}{N} trace(\left\langle (\hat{x}-x)(\hat{x}-x)^T \right\rangle P^{-1}) \end{aligned}$$

where N is the dimension of the state vector x, $\hat{x}$ is the track estimate, $\langle\ \rangle$ denotes empirical average, and P is the state error covariance estimated by the tracker. The covariance consistency will be approximately unity when the track covariance is close to the covariance P. The deviation of this quantity from unity gives rough measure of the overall track performance. Large covariance consistencies result in multiple platform track association failure, since the confidence regions for the tracks from each sensor will not intersect, as illustrated in Fig. 5. The track association problem is addressed by inflating the covariance matrix by an elevation dependent term that includes imprecise knowledge of the refraction correction.

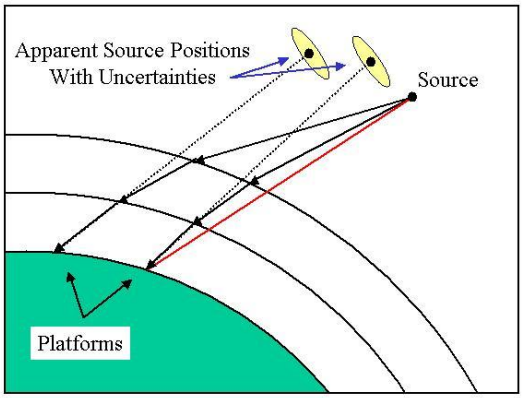

Fig. 5 Refraction effects at low elevation can be larger than measurement covariances, resulting in mis-association of tracks.

Fig. 6 shows the simulation results for covariance consistency for various bias inflation levels and refraction correction conditions. The CC curve marked by triangles (Δ) shows track results when refraction effects are absent from the simulation. The curve marked by circles ($\circ$) shows CC results for no bias covariance inflation and no refraction correction. The curve marked by squares ($\square$) shows the case of bias covariance inflation and no refraction correction. The curve marked by pluses (+) shows the CC history with no bias covariance inflation and 90% refraction correction. The curve marked by crosses (x) shows the CC for bias covariance inflation and 90% refraction correction.

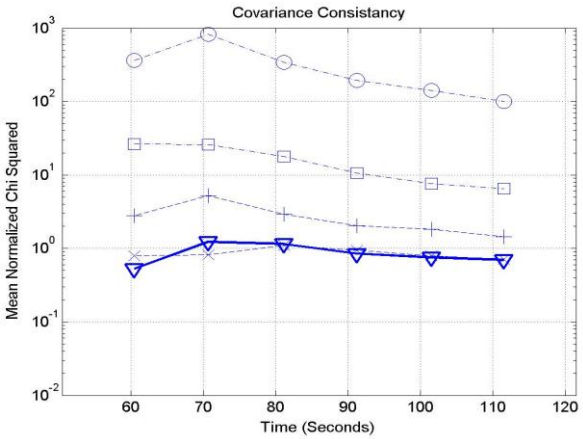

Fig. 6 Covariance consistency for various levels of refraction correction levels and bias covariance inflation.

As seen here, bias covariance inflation does lead to better covariance consistency, although in the case of no refraction correction, CC values are still an order of magnitude larger than desired.

IV. CONCLUSIONS

Approximations were derived for delay and bending of a waveform propagating through a spherically symmetric atmosphere with exponential decay of refractivity. These approximations are easily calculated and demonstrate good agreement with numerical ray tracing. The approximations were compared with the 4/3 Earth model in a common height finding application, where the two models showed comparable performance at very low elevation. The delay and bending results derived here exhibited better scaling with target elevation than the 4/3 Earth model due to the choice of the small parameter used in development of the approximations. A model based on these approximations was implemented in a computer simulation to illustrate the impacts of the refraction on tracking performance. The impacts of refraction on multiplatform multitarget track association were also discussed.

IV. REFERENCES

[1] Skolnik, Merrill: "Radar Handbook, Second Edition," McGraw-Hill Inc., New York, 1990, chap. 20.

[2] Barton, David K., and Ward, Harold R., "Handbook of Radar Measurement," Artech House, Inc., Dedham MA, 1984, Appendix D

[3] Feynman, Leighton, and Sands: "The Feynman Lectures on Physics," Addison-Wesley Publishing Co., Reading MA., 1963, vol 1, chap 26, vol 2, chap. 19.